A PWM Current-Source Converter-Based Wind Energy Conversion System

Ling Xing, Qiang Wei, *Senior Member, IEEE*, and Yunwei Li, *Fellow, IEEE*

***Abstract*—Current-source converters (CSCs) are a good candidate for the series-connected wind energy conversion system (WECS). However, the existing CSCs either exhibit poor generator stator current harmonics, require bulky low-frequency transformers, are limited in their application to synchronous generator-based wind systems, or necessitate complicated modulation and commutation. In this work, a new CSC is proposed and investigated. It features a unique hybrid structure consisting of a modular medium-frequency transformer-based voltage-source converter on the generator side and a conventional CSC on the grid side. The proposed converter offers superior generator stator current harmonics performance, a smaller size, simplified modulation and commutation schemes, and suitability for both synchronous and induction generator-based wind systems compared with the existing converters. In addition, all the advantages of the existing CSC-based WECS are retained. The proposed converter is discussed and analyzed, its control scheme is introduced, and its performance is investigated by both simulations and experiments.**

***Index Terms*—Current-source converter (CSC), medium-frequency transformer (MFT), wind energy conversion system (WECS).**

I. Introduction

THE series-connected wind energy conversion system (WECS), as shown in Fig. 1, eliminates the bulky and costly offshore substation used in the existing wind systems. This results in significant reductions in cost, size, weight, and power loss of existing WECS [1], [2]. Both voltage-source converters (VSCs) and current-source converters (CSCs) have been proposed for the series-connected WECS. Compared with VSCs [3], [4], [5], [6], [7], [8], [9], [10], CSCs are considered a good candidate for the series-connected system due to their variable dc-link voltage operation and reliable short-circuit protection [11], [12], [13], [14], [15], [16], [17], [18].

One of the technical challenges of the series-connected wind system is that the generator furthest from the ground must withstand the high-voltage dc (HVdc), while generators with such a high insulation level are impractical. To address this challenge, transformers are used to isolate generators from the HVdc. Depending on the type of used transformers, the existing CSCs can be divided into low-frequency transformer (LFT) based CSCs [11], [12], [13], [14] and medium-frequency transformer (MFT) based CSCs [15], [16], [17], [18].

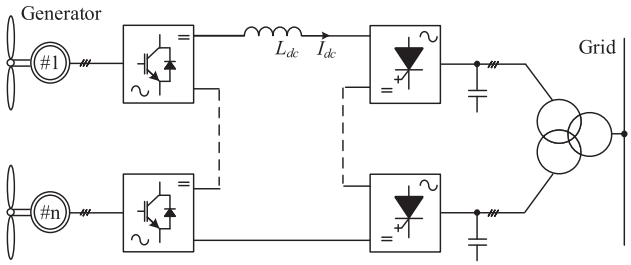

Fig. 1. Series-connected WECS.

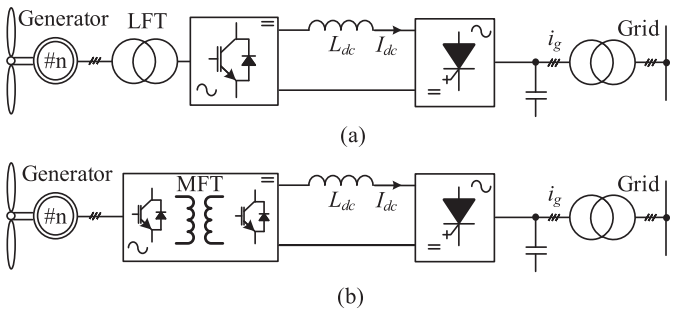

Fig. 2. Transformer-based CSCs. (a) LFT-based CSC. (b) MFT-based CSC.

Fig. 2(a) shows LFT-based CSCs where LFT is used on the generator side to isolate generators from high voltages. On the grid side, the conventional CSC is used. On the generator side, different converters were reported. In [11], a pulsewidth modulation (PWM) CSC is used on the generator side, while diode rectifier-based converters are employed in [12], [13], [14], and [25]. Compared with the PWM CSC, the use of passive rectifiers offers low cost and high reliability but suffers poor generator stator current harmonics performance. The LFT is a mature technology but features a large size and weight.

Fig. 2(b) shows MFT-based CSCs where MFT is used on the generator side to isolate generators from high voltages. The same as LFT-based CSCs, the conventional CSC is used on the grid side and different types of converters were proposed on the generator side. In [15], a single MFT-based converter was proposed for the generator-side converter of the CSC-based

Manuscript received 5 June 2023; revised 2 October 2023; accepted 11 November 2023. Date of publication 16 November 2023; date of current version 22 December 2023. Recommended for publication by Associate Editor M. Molinas. *(Corresponding author: Qiang Wei.)*

Ling Xing and Yunwei Li are with the Department of Electrical and Computer Engineering, University of Alberta, Edmonton, AB T6G 2R3, Canada (e-mail: lxing1@ualberta.ca; yunwei.li@ualberta.ca).

Qiang Wei is with the Department of Electrical Engineering, Lakehead University, Thunder Bay, ON P7B 5E1, Canada (e-mail: qwei@lakeheadu.ca).

Color versions of one or more figures in this article are available at https://doi.org/10.1109/TPEL.2023.3333315.

Digital Object Identifier 10.1109/TPEL.2023.3333315

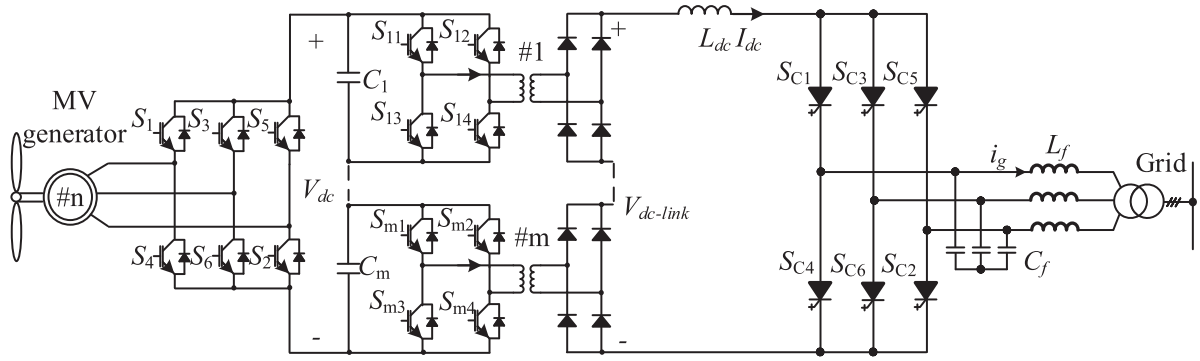

Fig. 3. Proposed CSC.

system. It is expected to have a smaller size and weight than the LFT, but the MFT with a high-power rating and a high insulation level is not mature technology. To address this challenge, a modular MFT-based converter was proposed in [16] and [17]. Thanks to the modular structure, each MFT carries partial power, reducing the manufacturing burden of MFT. However, the converters proposed in [15], [16], and [17] are all passive rectifier-based ones with highly distorted generator stator currents. To solve this problem, a matrix converter was proposed for the CSC-based wind system [18]. The matrix converter offers superior generator stator current harmonics performance but has a couple of drawbacks. For example, it operates as a CSC, requiring a high number of switches and complicated modulation, commutation, and control schemes. What is more, the lack of dc capacitors does not benefit the WECS, particularly under faults in which dc capacitors can help temporarily store the energy [19]. To sum up, the existing CSCs either are bulky, have poor generator stator current harmonics performance, or need complicated modulation and commutation schemes. The objective of this work is to develop a new CSC that solves the aforementioned challenges of the existing CSCs while retaining all their advantages.

In this work, a new CSC is proposed. It is a unique hybrid converter composed of an active VSC connected to an MFT-based modular converter on the generator side and a conventional CSC on the grid side. Its operation principle is discussed, and its control schemes are developed. It features a small size and weight and offers superior generator stator current harmonics, and it does not require complicated modulation and commutation schemes. In addition, all the advantages of existing CSCs are retained. The performance of the proposed converter and control scheme is investigated by simulations and experiments.

II. Proposed CSC-Based WECS

A. Proposed CSC

Fig. 3 shows the proposed medium-voltage CSC. It has a unique structure consisting of a two-stage VSC on the generator side and a CSC on the grid side. A modular MFT-based converter connected to a conventional two-level VSC is used on the generator side and a conventional CSC is used on the grid side. The modular MFT-based converter is composed of m identical H-bridge converters connected in series at both input and output. The MFTs are used to isolate the generator from high voltage to allow the use of generators with regular insulation levels. The modular structure of the MFT-based converter allows the use of cost-effective low-voltage devices and enables each MFT to carry $1/m$ of rated power, reducing the manufacturing burden of MFT. Depending on the power and voltage ratings of each wind turbine-generator unit, the conventional two-level VSC can be replaced with different ones, such as netrual point clamped (NPC). For example, the three-level NPC is a good candidate for medium-voltage generator systems. In this work, the optimization and comparison between different types of active rectifiers are not the focus. Instead, a conventional two-level VSC is used as a case study. On the grid side, the conventional CSC is used. It features reliable short-circuit protection and variable dc-link voltage operation, a good candidate for the series-connected wind system.

One of the advantages of the proposed converter is that its converter design can follow the existing ones. For example, the design of the generator-side two-level VSC, including switch selection, filter design, and dc voltage reference selection, is the same as the existing three-phase two-level VSC used in WECS. Refer to [19] for more details. The grid-side current CSC, along with passive components, such as the dc inductor and output LC filter, is designed in the same manner as the existing grid-connected CSCs [20], [21], [22], [23], [24]. For example, applying the voltage-second principle to the dc inductor can obtain the required dc inductance. In this case study, a 1-MW 4160-V CSC is studied, and the dc inductance needed is 45 mH. After the parameters of generator-side two-level VSC and grid-side CSC are determined, the parameters of the modular MFT-based converters can be determined accordingly. For example, when the 1700-V IGBT is selected, the number of modules (m) can be determined. The main function of MFTs is to isolate generators. As a result, the turn ratio of each MFT is 1:1, while its optimization is not a focus.

B. Discussions

The proposed CSC solves all technical challenges of the existing CSCs while retaining all their advantages.

Comparison with LFT-based CSCs: In the existing LFT-based CSCs, the LFT used is bulky and heavy, posing a burden due

to limited space in the nacelle. On the other hand, the MFT is smaller and lighter [28], providing significant benefits for wind systems, particularly offshore wind systems. However, the MFT used in the proposed WECS is high-power and high-voltage insulated, which is considered an immature technology. To address this issue, a modular MFT-based converter is introduced in which each MFT carries a portion of the rated power. This approach reduces the manufacturing burden of MFTs and positions the proposed modular MFT-based CSC as a promising candidate for series-connected wind systems.

Comparison with MFT-based CSCs with passive rectifiers: Diode rectifier-based CSCs feature low cost and complexity, as well as high reliability and scalability. However, they have two main drawbacks. First, they result in highly distorted generator stator currents, leading to increased losses, high torque ripples, and a shortened service timespan of generators [19], [27]. Second, they are limited to synchronous generator-based wind systems and cannot be used in induction generator-based wind systems [19]. In the proposed CSC, an active rectifier is utilized, offering superior harmonics performance. Furthermore, it can be applied to both induction generator- and synchronous generator-based wind systems. In additon, it can be extended for use in wind systems with different ratings by replacing the two-level VSC in this case study with different converters, such as NPC, cascaded H-bridge (CHB), and others. Although the proposed CSC using an active rectifier is more expensive and requires more complicated control compared with diode rectifier-based CSCs, it is a well-proven technology in the industry.

Comparison with MFT-based CSCs with active rectifiers: In the existing active rectifier-based CSCs, a matrix converter is utilized. However, it operates as a CSC, which necessitates intricate modulation and commutation schemes [18]. Moreover, this operation mode demands the use of switches with reverse voltage blocking capability, resulting in the adoption of more expensive and less efficient bidirectional switches [27]. In additon, the absence of dc capacitors in the matrix converter proves to be a disadvantage for wind systems. Conversely, the proposed converter incorporates the use of dc capacitors, providing the advantage of facilitating fault transitions in wind systems. Therefore, the proposed converter overcomes these drawbacks by offering simplified modulation and commutation schemes while utilizing cost-effective unidirectional switches. Furthermore, the inclusion of dc capacitors greatly aids in fault management in wind systems. Consequently, the proposed converter presents a favorable solution for the enhancement of active rectifier-based CSCs.

Efficiency: Under rated conditions with a hard switching technique and a switching frequency of several hundred hertz, the estimated efficiency breakdown of the proposed power converter is generator-side VSC = 99% [26], modular H-bridge converter = 99% [27], MFT = 99.3% [28], dc-link inductor = 98% [29], and grid-side CSC = 98.8% [29]. This leads to an overall efficiency of approximately 94%. The efficiency of the LFT-based CSC is slightly lower than that of the proposed CSC. This is primarily due to the lower efficiency of the LFT, which typically ranges from 95% to 98%, whereas in the proposed CSC, the MFT is expected to achieve a higher efficiency of

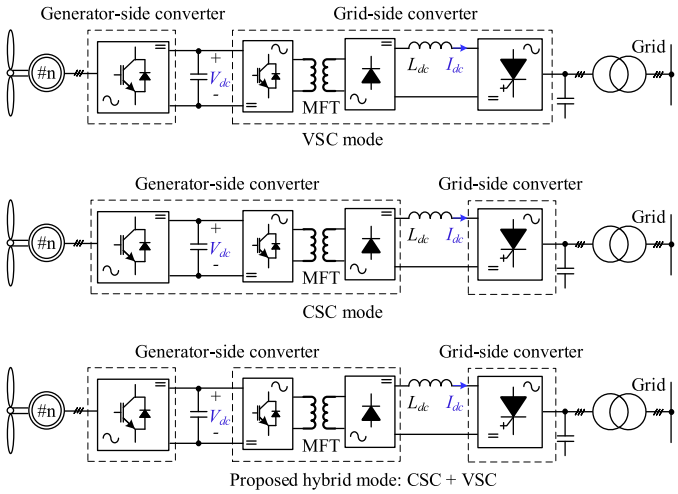

Fig. 4. Simplified circuit of the converter under VSC and CSC modes.

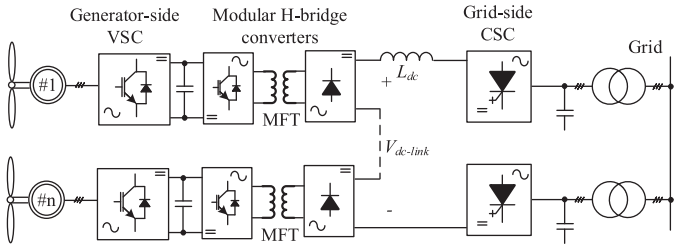

Fig. 5. Series-connected wind system consisting of the proposed CSCs.

99.3% [28]. On the other hand, the MFT-based CSC with a passive rectifier can achieve a higher efficiency of around 95%, thanks to the use of a passive rectifier rather than the active rectifier in the proposed converter. The existing MFT-based CSC with an active rectifier exhibits a similar efficiency performance to the proposed CSC.

III. Proposed Control Scheme

The proposed CSC has a unique structure consisting of a two-stage VSC on the generator side and a CSC on the grid side. Theoretically, it can operate as either a VSC or a CSC. In the VSC mode, as shown in Fig. 4, the voltage V_{dc} is controlled to remain constant, while the modular MFT-based converter and the grid-side CSC function as a grid-side converter where the current I_{dc} is variable. In the CSC mode, the dc-link current I_{dc} is controlled as a constant, while the modular MFT-based converter and the two-level VSC function as the generator-side converter where the voltage is V_{dc} variable. The CSC mode allows the series-connected wind system, consisting of the proposed converters, as shown in Fig. 5, to retain unique advantages, such as reliable short-circuit protection and variable dc voltage operation. On the other hand, the VSC mode simplifies the control system design of the generator-side converter, including the two-level VSC and the modular MFT-based converter for each turbine-generator unit. Therefore, to ensure the benefits of both the series-connected wind system and the power converter

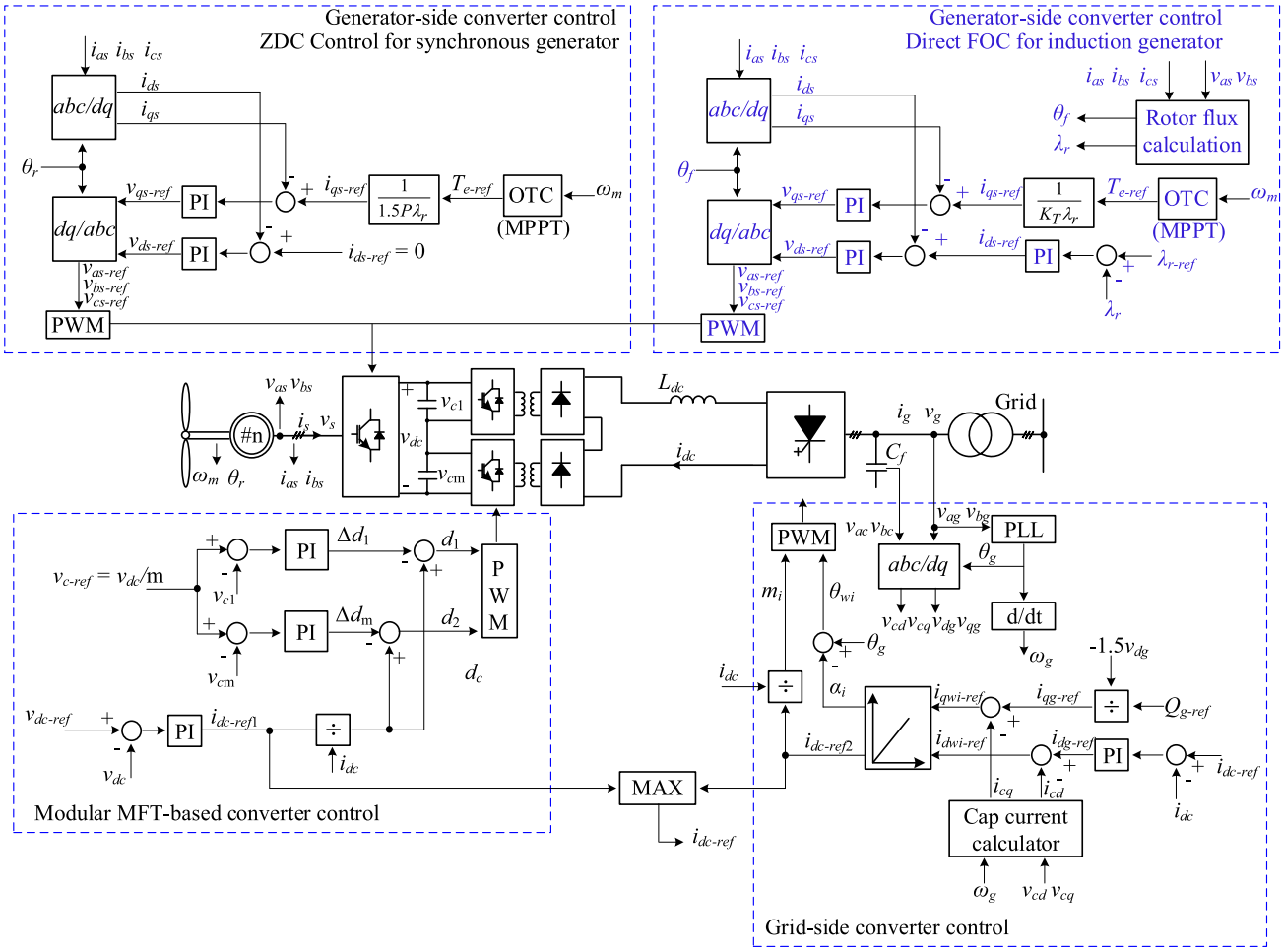

Fig. 6. Proposed hybrid control of the proposed converter.

for each turbine-generator unit, a hybrid control scheme that combines the CSC and VSC modes is proposed.

The hybrid control scheme is illustrated in Fig. 6 and includes three parts: generator-side control, grid-side control, and the control of the modular MFT-based converter.

1) Generator-side controls: maximum power point tracking (MPPT) and generator speed control.
2) MFT-based modular converter controls: dc capacitor voltage control and voltage balancing of the modular converter.
3) Grid-side controls: dc-link current control and reactive power control.

A. Generator-Side Converter Controls

The generator-side converter controls the active wind power, while its output voltage, the dc voltage $V_{\rm dc}$ is controlled as a constant achieved by the control of the MFT-based converter. On this basis, the proposed converter is simplified and equivalent to the one, as shown in Fig. 7, in which a constant voltage source is used to represent the load of the generator-side VSC. In doing so, the existing generator controls can be applied directly [19].

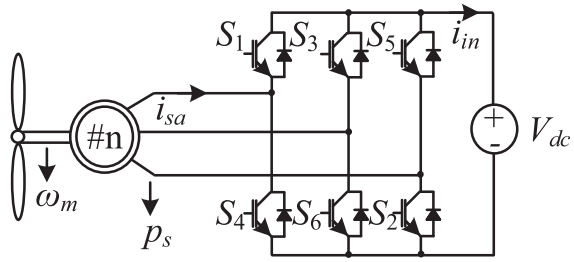

Fig. 7. Equivalent circuit for generator-side converter.

The use of the active rectifier allows the use of both synchronous generators and induction generators. In the following, controls for both types of generators are presented.

1) Synchronous generator control: All the well-proven controls, including the zero d-axis current control (ZDC), maximum torque per ampere control, and unity power factor control, can be applied to the proposed converter. In the following, the ZDC is taken as an example. As shown in Fig. 6, the MPPT is achieved by the optimal torque control (OTC) [19], and the generator is controlled by the ZDC [19]. According to the measured rotor speed ω_m,

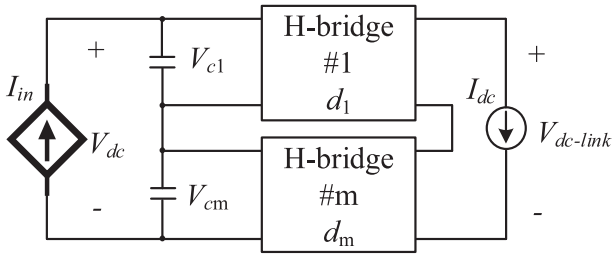

Fig. 8. Equivalent circuit for MFT-based modular converter.

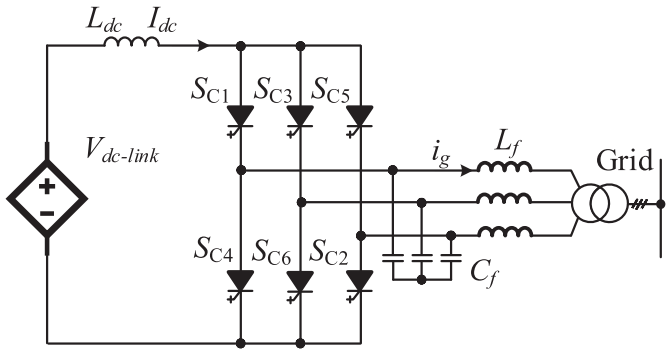

Fig. 9. Equivalent circuit for grid-side converter.

the OTC outputs the reference torque $T_{e\text{-ref}}$, which then gives the torque-producing stator current reference $i_{qs\text{-ref}}$. $i_{qs\text{-ref}}$ is calculated based on the ZDC scheme in which the d-axis stator current reference $i_{ds\text{-ref}}$ is set to 0

$$T_e = \frac{3}{2} P \lambda_r i_{qs} \tag{1}$$

where P is the pole pairs and λ_r is the rotor flux linkage.

The measured three-phase stator currents (i_{as}, i_{bs}, and i_{cs}) are transformed into the dq-axis currents (i_{ds} and i_{qs}), which are then compared with their respective reference currents ($i_{ds\text{-ref}}$ and $i_{qs\text{-ref}}$). The resultant errors are then sent to PI controllers, which generate the dq-axis reference voltages ($v_{ds\text{-ref}}$ and $v_{qs\text{-ref}}$) for the generator-side converter. The use of *dq/abc* transformation gives *abc*-frame reference voltages ($v_{as\text{-ref}}$, $v_{bs\text{-ref}}$, and $v_{cs\text{-ref}}$), which are then sent to the PWM generation block. In this study, a conventional sinusodial pulse width modulation (SPWM) is used, and in both *abc/dq* and *dq/abc* transformations, the rotor position angle θ_r is used. The stator voltages of the generator are then controlled according to their references such that the active power is controlled.

2) Induction generator control: The existing well-used controls, such as the direct field-oriented control (FOC), indirect FOC, and direct torque control, all can be used here directly. The direct FOC is taken as an example. As shown in Fig. 6, the implementation of the direct FOC is similar to that of the ZDC except that the direct FOC has one more control loop, the rotor flux control. The rotor flux controller outputs the d-axis stator current reference $i_{ds\text{-ref}}$, which, however, is set to zero in the case of ZDC. Other than this, the two controls are the same and, thus, not repeated. Refer to [19] for more details, including the comparison between different controls.

B. MFT-Based Modular Converter Controls

The MFT-based modular converter controls the dc voltage $V_{\rm dc}$ to be a constant in the full operation range. The dc current $I_{\rm dc}$ is controlled by the grid-side converter. Therefore, from the control system design perspective, the proposed converter is equivalent to the one, as shown in Fig. 8. The input of the MFT-based converter is represented by a voltage-controlled current source $I_{\rm in}$ and the output by a constant current source. Note that the constant current source has different values under different wind speeds, which will be discussed in the grid-side converter control. In addition, the modular structure of the MFT-based converter requires power balancing control. As shown in Fig. 8, all the modules share the same $I_{\rm dc}$ at the output, but there is a voltage imbalance issue due to parameters mismatch. For example, the turn ratio of all the transformers is set to 1:1, which, however, is not guaranteed due to the existence of tolerance. Then, the module with a higher turn ratio suffers a higher capacitor voltage. However, the structure of the series connection at both input and output is not stable upon a mismatch, and the voltage balancing control is needed.

As shown in Fig. 6, the measured dc voltage $V_{\rm dc}$ is compared with its reference $V_{\rm dc\text{-}ref}$ value. Note that the reference voltage $V_{\rm dc\text{-}ref}$ is selected as same as the existing VSC-based wind systems [19], thus not repeated here. The error is sent to the PI controller that generates the current reference $i_{\rm dc\text{-}ref1}$. The required duty cycle d_c for dc voltage control is then obtained by comparing the reference current $i_{\rm dc\text{-}ref1}$ and actual dc current $i_{\rm dc}$. Voltage balancing control is introduced to ensure voltage balancing. As shown in Fig. 6, the measured capacitor voltages v_{c1} and v_{cm} are compared with their reference values; and the errors then go through the PI controllers, respectively, to generate the required duty cycles for voltage balancing. The final duty cycle for each module includes two parts: d_c and Δd_m. The former is to ensure dc voltage control, while the latter ensures voltage balancing.

The dc current reference $i_{\rm dc\text{-}ref1}$ is physically referring to the generator-side dc current reference that is needed to achieve generator-side control objectives, including the MPPT and generator speed control as well as the dc voltage control and power balancing control. For example, with the dc current $i_{\rm dc}$ lower than this current reference $i_{\rm dc\text{-}ref1}$, the dc voltage control is not achieved, which, in turn, results in a failure of active power control. Therefore, this dc current reference $i_{\rm dc\text{-}ref1}$, as shown in Fig. 6, is sent to the grid-side converter for the dc current control.

C. Grid-Side Converter Controls

The grid-side converter is responsible for the dc current control and reactive power control. The simplified equivalent circuit is shown in Fig. 9 in which the input is represented by a current-controlled voltage source in series with the dc inductor. The control scheme is designed and shown in Fig. 6.

As shown in Fig. 6, the grid-side control includes two independent control loops in the *dq*-frame, one is the dc current control loop and the other is the reactive power control loop. The *d*-axis grid current reference ($i_{dg\text{-ref}}$) is obtained by the dc current PI controller. The reference for the *q*-axis grid current ($i_{qg\text{-ref}}$) is obtained according to the following reactive power reference ($Q_{g\text{-ref}}$) and the *d*-axis grid voltage (v_{dg})

$$Q_g = -\frac{3}{2} v_{dg} i_{qg}. \tag{2}$$

The references for the *dq*-axis converter PWM currents ($i_{dwi\text{-ref}}$ and $i_{qwi\text{-ref}}$) are calculated considering the capacitor currents of the grid-side converter with the relationship given as follows:

$$\begin{aligned} i_{dwi-\text{ref}} &= i_{dg-\text{ref}} - i_{cd} = i_{dg-\text{ref}} + \omega_g C_f v_{cq} \\ i_{qwi-\text{ref}} &= i_{qg-\text{ref}} - i_{cq} = i_{qg-\text{ref}} - \omega_g C_f v_{cd} \end{aligned} \tag{3}$$

where ω_g is the grid frequency, i_{cd} and i_{cq} are the *dq*-axis capacitor currents, and v_{cd} and v_{cq} are the *dq*-axis capacitor voltages.

The amplitude ($i_{\text{dc-ref}2}$) and delay angle (α_i) of the grid-side converter then can be calculated based on the Cartesian-to-polar transformation

$$\begin{aligned} i_{\text{dc}-\text{ref2}} &= \sqrt{(i_{dwi-\text{ref}})^2 + (i_{qwi-\text{ref}})^2} \\ \alpha_i &= \tan^{-1}(i_{qwi-\text{ref}}/i_{dwi-\text{ref}}). \end{aligned} \tag{4}$$

The required modulation index (m_i) for the converter is then obtained by dividing the PWM current reference ($i_{\text{dc-ref2}}$) by the dc current i_{dc}. And the required angle of the converter PWM current (θ_{wi}) is calculated based on $\theta_{wi} = \theta_g - \alpha_i$ in which θ_g is the grid voltage angle obtained based on the phase lock loop (PLL) block. After applying m_i and θ_{wi} to the grid-side converter, both reactive power and dc current are controlled.

Note that both the dc current reference ($i_{\text{dc-ref1}}$) generated by the generator-side control (including the MFT-based converter control) and the one ($i_{\text{dc-ref2}}$) generated by the grid-side control should be considered to determine the dc current reference ($i_{\text{dc-ref}}$). The larger one of the two references is selected to be the dc current reference $i_{\text{dc-ref}}$ such that the controls at both sides are achieved. Refer to [16], [17], and [18] for details of dc current reference determination.

In summary, compared with the existing CSC-based converters, the proposed control has an extra dc voltage control, while compared with the existing VSC-based converters, the proposed control has an extra dc current control. By applying the proposed control scheme, controls on both sides are achieved, and power balancing is ensured as well.

IV. Investigation of the Proposed Power Converter

Both MATLAB simulation and lab-scale experiments are conducted to study the performance of the proposed converter and control scheme. The used parameters are listed in Table I in which transformer turn ratios used in simulations are set to different purposely to simulate the mismatch in practice.

TABLE I
Simulation and Experimental Parameters

Parameters	Simulation	Experiment
Nominal power	1 MW	866 W
Grid voltage V_g	4160 V	110 V
Generator	PMSG, 4000 V	Variac
Generator-side converter		
Filter inductor L_g	20 mH	10 mH
DC voltage V_{dc}	8000 V	160 V
Switching frequency	2 kHz	2 kHz
MFT-based modular converter		
# of modules m	6	2
Transformer	6	2
Transformer turn ratio	1:1, 1:1.01, 1:1.02, 1:1.03, 1:1.04, 1:1.05	1:1, 1: 1 (Extra resistor $R_p = 600\ \Omega$)
Capacitor C_{m}	1000 μF	1000 μF
Switching frequency	1.2 kHz	1.2 kHz
Grid-side converter		
DC inductor L_{dc}	45 mH	45 mH
Filter inductor L_f	5 mH	5 mH
Filter capacitor C_f	70 μF	100 μF
Switching frequency	540 Hz	540 Hz

A. Simulated Results

Fig. 10 shows the simulated waveforms under both steady and dynamic states. Before $t = 1.5$ s, the converter is operating under rated conditions. At the generator side, the generator torque T_e is controlled at its reference value $T_{e\text{-ref}}$ obtained by the OTC, and both terminal voltage (v_{as}) and stator current (i_{as}) are at rated values. The controls of the MFT-based converter are also achieved. The dc voltage is controlled at 1 p.u. and it is evenly distributed among the capacitors ($v_{c1} = v_{c6}$). At the grid side, the dc current is controlled at its rated value and the real power and reactive power are controlled to be 1 and 0 p.u.

At $t = 1.5$ s, the voltage balancing control is removed. As a result, the capacitor voltages are starting to deviate due to the tolerance/mismatch of the used transformers. As discussed earlier, the modules with higher turn ratios are suffering higher capacitor voltages, and here that is v_{c1} that increases to 1.3 p.u., while v_{c1} decreases to around 0.75 p.u. At $t = 2$ s, the voltage balancing control is switched in, and as a result, the capacitor voltages are tracking their reference values and go back to the balance again. During this period of time, the generator-side controls, as shown in Fig. 10(a), the grid-side controls, as shown in Fig. 10(c), and the dc voltage control of the MFT-based converter, as shown in Fig. 10(b), are achieved.

At $t = 2.5$ s, the generated reference torque $T_{e\text{-ref}}$ starts to decrease from -1 down to -0.5 p.u. at $t = 2.75$ s, and then is kept constant. With the proposed control, its actual torque is tracking well with the reference torque, the generated terminal voltage (v_{as}) and current (i_{as}) at the generator side decrease accordingly, the dc voltage (v_{dc}) is kept constant under control and the capacitor voltages are well balanced under control, and the captured real power (p_g) decreased from 1 to around 0.25 p.u. at the grid side accordingly. The dc current (i_{dc}) is well tracking its reference $i_{\text{dc-ref}}$ that is reduced from 1 to around 0.58 p.u.

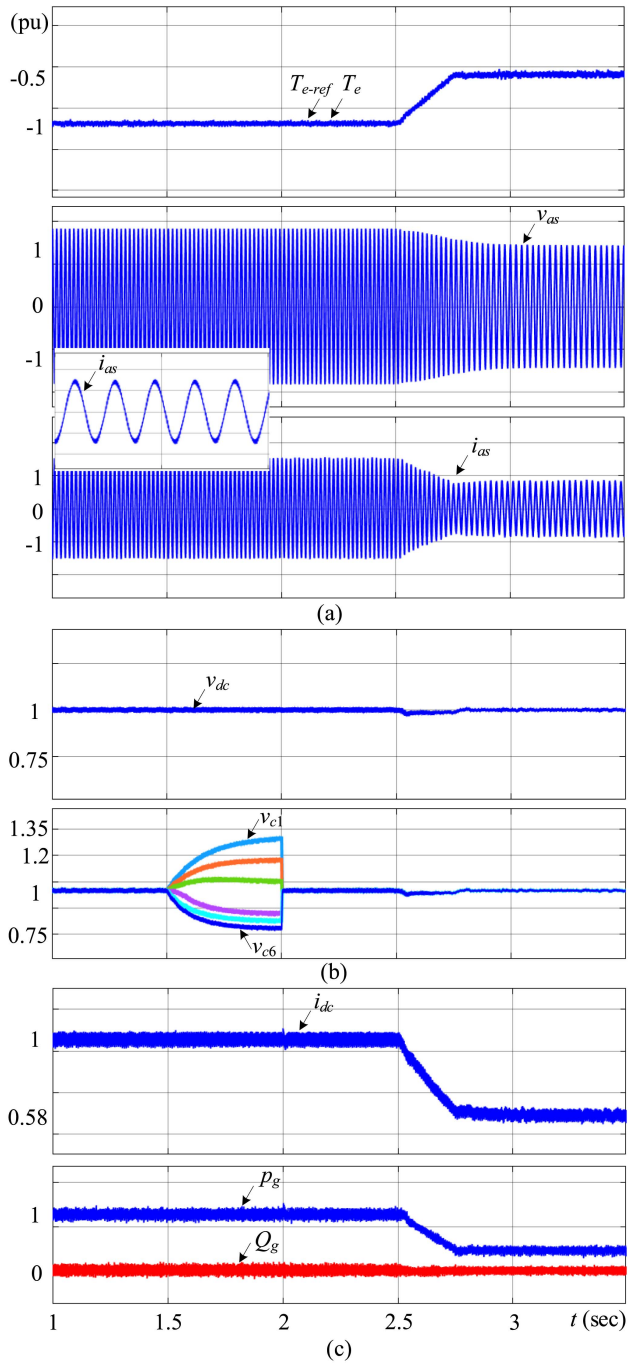

Fig. 10. Simulated waveforms under steady and dynamic states synchronous generator. (a) Waveforms of generator-side converter. (b) Waveforms of MFT-based converter. (c) Waveforms of grid-side converter.

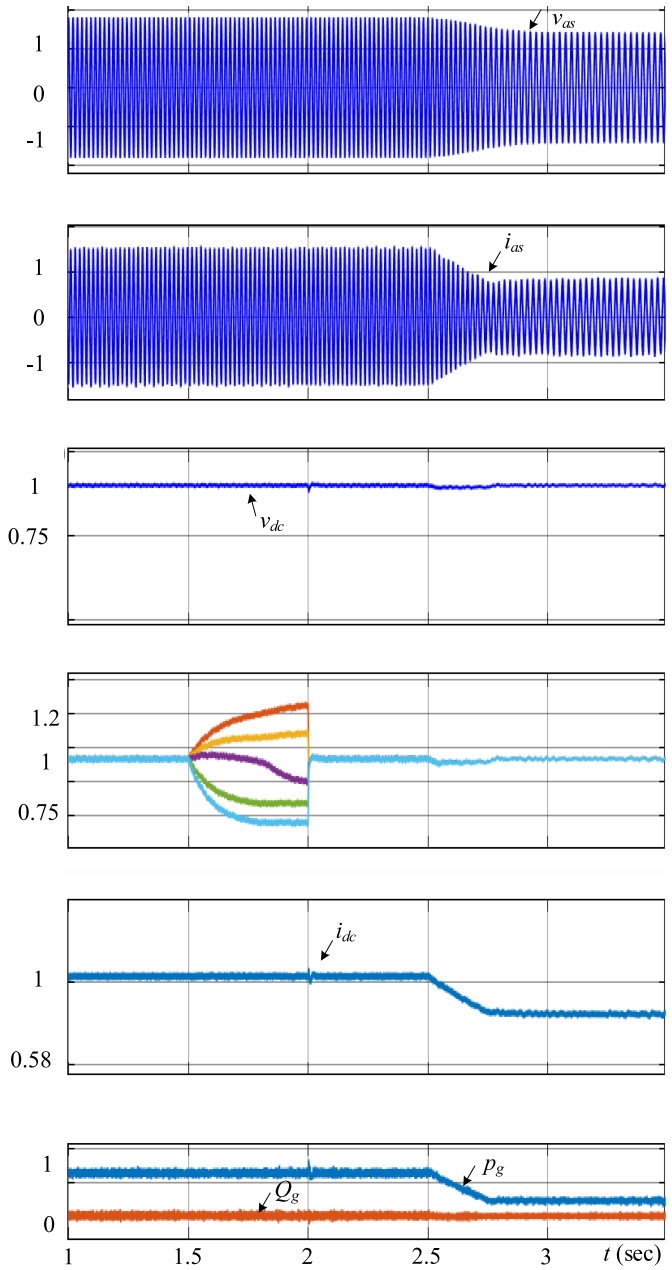

Fig. 11. Simulated waveforms under steady and dynamic states induction generator.

to lower power loss as well as ensure the grid-side control. The reactive power is controlled to 0 achieving a unity power factor at the grid side. To sum up, the above-simulated results verify the effectiveness of the proposed control scheme in achieving these defined control objectives.

Fig. 11 shows the simulated results of the power converter when used for an induction generator wind system under the same conditions as the synchronous generator wind system. As discussed earlier, the only difference between the synchronous generator and induction generator wind systems is the generator control, while the proposed power converter's performance remains the same. As shown in Fig. 11, the waveforms of the proposed converter fed by an induction generator are the same as those in Fig. 10 under the same conditions. The details of the waveforms are not repeated here.

Fig. 12 shows the simulated waveforms during the startup of the permanent magnet synchronous generator (PMSG) wind system. At $t = 0.1$ s, the generator torque T_e starts to increase following its reference up to its rated value at $t = 0.6$ s and is then kept constant. The rotor speed ω_m changes in the same manner. At $t = 0.6$ s, it reaches the rated speed. The generator outputs, including the phase voltage (v_{as}) and current

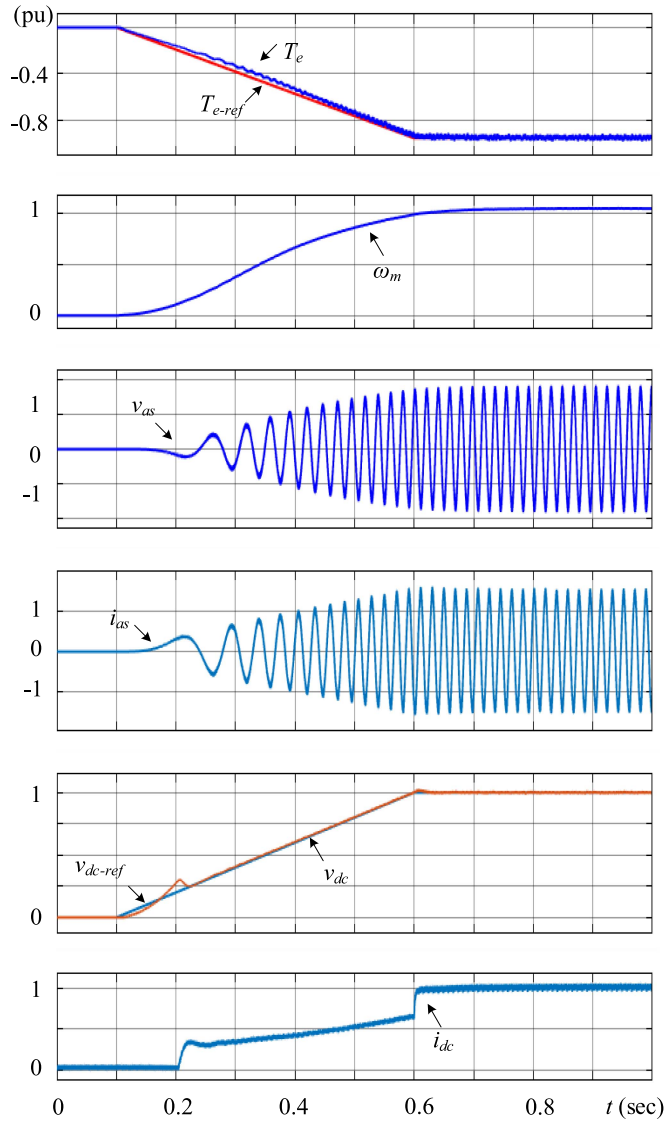

Fig. 12. Simulated waveforms of the proposed converter during startup.

(i_{as}), are also illustrated in Fig. 12. During the startup, the voltage $V_{\rm dc}$ of the generator-side converter is controlled to track its reference value $V_{\rm dc\text{-}ref}$, which is set in proportion to the generator rotor speed. The dc-link current $I_{\rm dc}$ during the startup is controlled differently. During the startup, that is before $t = 0.6$ s, in which the rotor speed is not reaching its rated value and the captured power is low, the dc-link current reference is set to a lower value. At $t = 0.6$ s, the system reaches its rated conditions and the $I_{\rm dc}$ starts to be controlled to follow its rated value. It is worth noting that different control scenarios can be applied to the startup. The one illustrated here is an example.

As analyzed earlier, one of the advantages of the proposed CSC is its superior generator stator current harmonics performance over the conventional diode rectifier-based CSC [16]. Fig. 13 shows the simulated waveforms of stator current and its harmonics profile of the two types of CSC under rated conditions. As shown in Fig. 13, the proposed CSC has a much better harmonics performance of a total harmonic distortion (THD) of

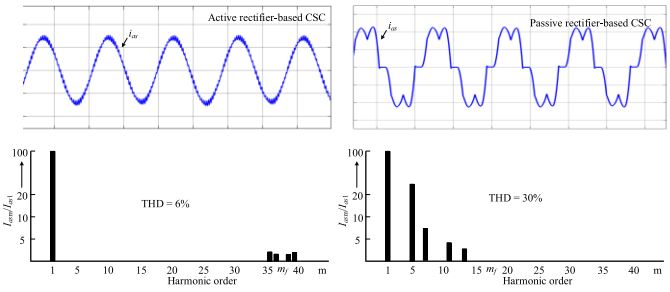

Fig. 13. Simulated harmonics performance of active rectifier- and passive rectifier-based CSCs.

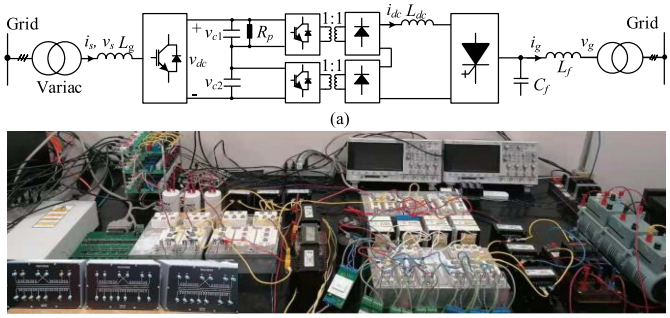

Fig. 14. Lab-scale experimental setup. (a) Circuit of the experimental setup. (b) Photograph of the experimental setup.

around 6%, while it is 30% for the diode rectifier-based CSC [16].

B. Experimental Results

A down-scale setup, as shown in Fig. 14, is built to verify the performance of the proposed converter and control. As shown in Fig. 14, a variac is used to function the turbine-generator set, a transformer is used at the grid to step up the output voltage to the grid voltage level, and an extra resistor ($R_p = 600\ \Omega$) is used to introduce voltage imbalance of the MFT-based converter. The parameters are listed in Table I.

Fig. 15 shows the experimental waveforms of the proposed converter under both steady state and dynamic state. Fig. 15(a) and (b) shows the steady-state performance of the proposed converter under rated condition in which the generator-side voltage V_s (line-to-line voltage) = 71 V and the grid-side voltage V_g (line-to-line voltage) = 104 V. As shown in Fig. 15(a), the generator-side current i_{as} (phase current) = 7.1 A is well controlled under steady state. The phase displacement between V_s and i_{as} is 30°, which indicates a unity power factor at the generator side. The dc voltage ($V_{\rm dc} = 160$ V) and the dc current ($I_{\rm dc} = 6.5$ A) are all well controlled to be their respective references. Fig. 10(b) shows the steady-state waveforms of the grid voltage and the grid current under the same rated condition. As shown in the figure, the grid voltage V_g (line-to-line voltage) = 104 V and the grid current i_{ag} (phase current) = 4.3 A under a unity power factor control ($Q_{g\text{-ref}} = 0$) are well achieved under steady state.

Fig. 15(c)–(e) shows the experimental waveforms under dynamic state. For the wind system where a turbine-generator

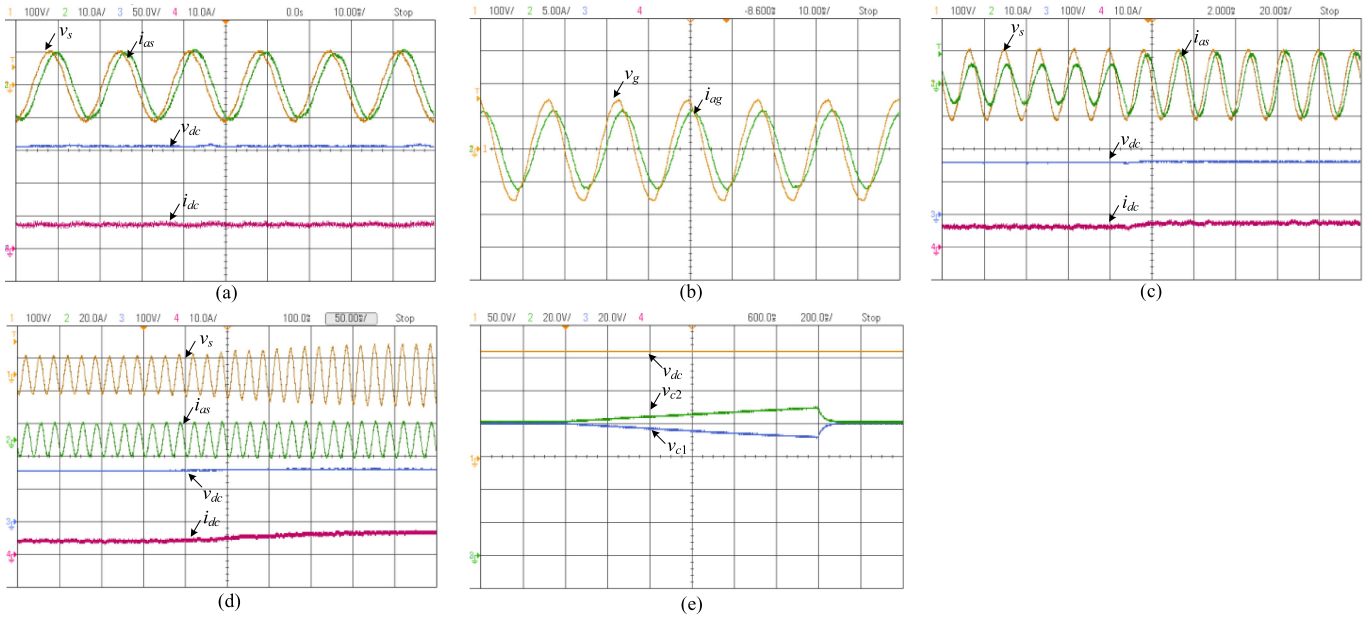

Fig. 15. Experimental waveforms of the proposed hybrid CSC. (a) Generator-side voltage and current and the dc-link voltage and current under steady state. (b) Grid-side voltage and current under steady state. (c) Generator-side voltage and current and the dc-link voltage and current under dynamic state. (d) Generator-side voltage and current and the dc-link voltage and current under dynamic state. (e) Capacitor voltage under dynamic state.

set is used, the generator-side voltage and current are changed at the same time under wind speed change. Since a variac is used in the experiments to simulate the turbine-generator set, its voltage and current cannot be changed at the same time. Therefore, two experiments are conducted, one is with constant generator-side voltage V_s, while the generator-side current i_{as} is changed, and the other is with constant generator-side current, while the generator-side voltage is changed. Fig. 15(c) shows the performance under a stepped change of i_{as} in which i_{as} is controlled to step from 3.5 to 7 A. Under such a change, the dc voltage $v_{\rm dc} = 160$ V is well ensured, and the dc current $I_{\rm dc}$ is changed accordingly to ensure both control objectives at both generator and grid sides. Similarly, as shown in Fig. 15(d) in which i_{as} is kept at 7 A, while the V_s is increased from around 35 to 70 V by manually regulating the variac, the dc voltage control ensures $V_{\rm dc} = 160$ V, and the dc current control gives a corresponding change. Fig. 15(e) shows the performance of the voltage balancing control under both steady and dynamic states. As shown in the figure, with the balancing control, $V_{c1} = V_{c2}$ is ensured, while without the balancing control, a voltage deviation occurs. V_{c1} is decreased while V_{c2} is increased due to the use of the extra resistor R_p. To sum up, the above simulated and experimental results well verify the performance of the proposed converter and the proposed control scheme.

Fig. 16 shows the experimental harmonic profile of the stator current i_{as}. As shown in the figure, compared with the diode rectifier-based CSC [16] where the stator current is highly distorted, the stator current harmonics performance of the proposed active rectifier-based CSC is significantly improved. Note that the experimental THD (around 9%) is slightly higher than the simulated value (6%). The active rectifier offers superior current harmonics performance, and it is a well-proven conclusion, refer to [27] for more.

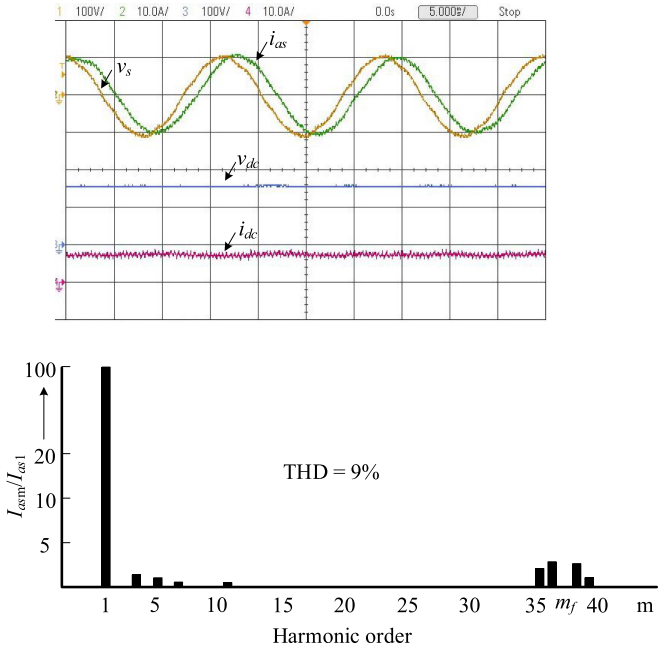

Fig. 16. Harmonics profile of the experimental current.

V. Conclusion

A new power converter is proposed and investigated for the CSC-based WECS. It features a unique hybrid structure comprising an active VSC connected to a modular MFT-based converter on the generator side, as well as a CSC on the grid side. This unique hybrid structure necessitates the proposal of a hybrid control scheme. In comparison to the existing CSC-based systems, the proposed converter employs an additional dc voltage control, while compared with the existing VSC-based

systems, it introduces an extra dc current control. In additon, a voltage balancing scheme is adapted for the modular MFT-based converter. Simulation and experimental studies have been conducted to verify the performance of the proposed converter and the effectiveness of the control scheme. The results demonstrate that the proposed CSC outperforms existing LFT-based CSCs in terms of size and weight, thanks to the utilization of modular MFTs. Compared with the existing MFT-based CSCs with passive rectifiers, the proposed CSC offers superior performance in generator stator current harmonics, resulting in reduced losses, low torque ripples, and an extended service lifespan for generators. Moreover, the proposed CSC is suitable for both synchronous and inductor generator-based wind systems, whereas passive rectifier-based CSCs can only be used with synchronous generators. Unlike MFT-based CSCs with active rectifiers, the proposed CSC eliminates the need for complicated modulation and commutation schemes. In additon, the cost and complexity associated with switches are reduced since the generator-side converter does not require bidirectional switches, which are needed in the existing ones.

REFERENCES

[1] M. Guan, "A series-connected offshore wind farm based on modular dual-active-bridge (DAB) isolated DC–DC converter," *IEEE Trans. Energy Convers.*, vol. 34, no. 3, pp. 1422–1431, Sep. 2019.

[2] T. H. Nguyen, D.-C. Lee, and C.-K. Kim, "A series-connected topology of a diode rectifier and a voltage-source converter for an HVDC transmission system," *IEEE Trans. Power Electron.*, vol. 29, no. 4, pp. 1579–1584, Apr. 2014.

[3] G. Guo et al., "Series-connected-based offshore wind farms with full-bridge modular multilevel converter as grid- and generator-side converters," *IEEE Trans. Ind. Electron.*, vol. 67, no. 4, pp. 2798–2809, Apr. 2020.

[4] G. Guo et al., "HB and FB MMC based onshore converter in series-connected offshore wind farm," *IEEE Trans. Power Electron.*, vol. 35, no. 3, pp. 2646–2658, Mar. 2020.

[5] F. Rong, G. Wu, X. Li, S. Huang, and B. Zhou, "ALL-DC offshore wind farm with series-connected wind turbines to overcome unequal wind speeds," *IEEE Trans. Power Electron.*, vol. 34, no. 2, pp. 1370–1381, Feb. 2019.

[6] M. Pape and M. Kazerani, "A generic power converter sizing framework for series-connected DC offshore wind farms," *IEEE Trans. Power Electron.*, vol. 37, no. 2, pp. 2307–2320, Feb. 2022.

[7] C. Meyer, M. Hoing, A. Peterson, and R. W. De Doncker, "Control and design of DC grids for offshore wind farms," *IEEE Trans. Ind. Appl.*, vol. 43, no. 6, pp. 1475–1482, Nov./Dec. 2007.

[8] N. Holtsmark, H. J. Bahirat, M. Molinas, B. A. Mork, and H. K. Hoidalen, "An all-DC offshore wind farm with series-connected turbines: An alternative to the classical parallel AC model?," *IEEE Trans. Ind. Electron.*, vol. 60, no. 6, pp. 2420–2428, Jun. 2013.

[9] A. Garcés and M. Molinas, "A study of efficiency in a reduced matrix converter for offshore wind farms," *IEEE Trans. Ind. Electron.*, vol. 59, no. 1, pp. 184–193, Jan. 2012.

[10] Z. Wang, B. Yuwen, Y. Lang, and M. Cheng, "Improvement of operating performance for the wind farm with a novel CSC-type wind turbine-SMES hybrid system," *IEEE Trans. Power Del.*, vol. 28, no. 2, pp. 693–703, Apr. 2013.

[11] R. E. Torres-Olguin, A. Garces, M. Molinas, and T. Undeland, "Integration of offshore wind farm using a hybrid HVDC transmission composed by the PWM current-source converter and line-commutated converter," *IEEE Trans. Energy Convers.*, vol. 28, no. 1, pp. 125–134, Mar. 2013.

[12] S. Nishikata and F. Tatsuta, "A new interconnecting method for wind turbine/generators in a wind farm and basic performances of the integrated system," *IEEE Trans. Ind. Electron.*, vol. 57, no. 2, pp. 468–475, Feb. 2010.

[13] M. Popat, B. Wu, F. Liu, and N. Zargari, "Coordinated control of cascaded current-source converter based offshore wind farms," *IEEE Trans. Sustain. Energy*, vol. 3, no. 3, pp. 557–565, Jul. 2012.

[14] E. Veilleux and P. W. Lehn, "Interconnection of direct-drive wind turbines using a series-connected DC grid," *IEEE Trans. Sustain. Energy*, vol. 5, no. 1, pp. 139–147, Jan. 2014.

[15] Y. Xia, K. H. Ahmed, and B. W. Williams, "A PWM current source-based DC transmission system for multiple wind turbine interfacing," *IEEE J. Emerg. Sel. Topics Power Electron.*, vol. 2, no. 4, pp. 784–796, Dec. 2014.

[16] Q. Wei, B. Wu, D. Xu, and N. R. Zargari, "A medium-frequency transformer-based wind energy conversion system used for current-source converter-based offshore wind farm," *IEEE Trans. Power Electron.*, vol. 32, no. 1, pp. 248–259, Jan. 2017.

[17] Q. Wei, B. Wu, D. Xu, and N. R. Zargari, "A new configuration using PWM current source converters in low-voltage turbine-based wind energy conversion systems," *IEEE J. Emerg. Sel. Topics Power Electron.*, vol. 6, no. 2, pp. 919–929, Jun. 2018.

[18] Y. Xu, Z. Wang, P. Liu, Q. Wei, F. Deng, and Z. Zou, "The modular current-fed high-frequency isolated matrix converters for wind energy conversion," *IEEE Trans. Power Electron.*, vol. 37, no. 4, pp. 4779–4791, Apr. 2022.

[19] B. Wu, Y. Lang, N. Zargari, and S. Kouro, *Power Conversion and Control of Wind Energy Systems*. Hoboken, NJ, USA: Wiley, 2011.

[20] J. He, Q. Li, H. Wang, Y. Lyu, H. Jia, and C. Wang, "SVM strategies for simultaneous common-mode voltage reduction and DC current balancing in parallel current source converters," *IEEE Trans. Power Electron.*, vol. 33, no. 10, pp. 8859–8871, Oct. 2018.

[21] X. Guo, D. Xu, J. M. Guerrero, and B. Wu, "Space vector modulation for DC-link current ripple reduction in back-to-back current-source converters for microgrid applications," *IEEE Trans. Ind. Electron.*, vol. 62, no. 10, pp. 6008–6013, Oct. 2015.

[22] P. Liu, Z. Wang, Q. Song, Y. Xu, and M. Cheng, "Optimized SVM and remedial control strategy for cascaded current-source-converters-based dual three-phase PMSM drives system," *IEEE Trans. Power Electron.*, vol. 35, no. 6, pp. 6153–6164, Jun. 2020.

[23] L. Ming, W. Ding, P. C. Loh, and Z. Xin, "A direct carrier-based modulation scheme with full index range for DC-link current ripple mitigation of a current source converter," *IEEE Trans. Ind. Electron.*, vol. 69, no. 1, pp. 452–462, Jan. 2022.

[24] Z. Bai, H. Ma, D. Xu, B. Wu, Y. Fang, and Y. Yao, "Resonance damping and harmonic suppression for grid-connected current-source converter," *IEEE Trans. Ind. Electron.*, vol. 61, no. 7, pp. 3146–3154, Jul. 2014.

[25] L. Xing, Q. Wei, and Y. Li, "A new power converter for current source converter-based wind energy system," *IEEE Trans. Ind. Electron.*, vol. 69, no. 12, pp. 12851–12858, Dec. 2022.

[26] ABB Wind Turbine Converters, 2023. [Online]. Available: https://search.abb.com/library/Download.aspx?DocumentID=3BHS351272&LanguageCode=en&DocumentPartId=&Action=Launch

[27] B. Wu, *High-Power Converters and AC Drives*. New York, NY, USA: Wiley, 2006.

[28] Shrinking the Core, 2023. [Online]. Available: https://library.e.abb.com/public/aa540228f875a641c1257ab8003ae5e7/37-40%20sr108_72dpi.pdf

[29] PowerFlex Medium Voltage AC Drives, 2023. [Online]. Available: https://rexel-cdn.com/Products/0809A6E2-B22C-44C7-9C78-0F3F1F991B04/0809A6E2-B22C-44C7-9C78-0F3F1F991B04.pdf

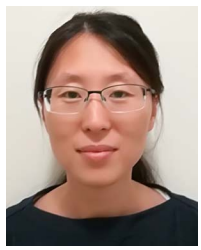

Ling Xing received the B.Sc. degree from Harbin Institute of Technology, Harbin, China, in 2009, and the M.A.Sc. degree from Xi'an Jiaotong University, Xi'an, China, in 2012, both in electrical engineering. She is currently working toward the Ph.D. degree in power engineering with the Department of Electrical and Computer Engineering, University of Alberta, Edmonton, AB, Canada.

Her research interest focuses on high-power converters in renewable energy systems.

Qiang Wei (Senior Member, IEEE) received the B.Sc. degree from Henan University of Science and Technology, Luoyang, China, in 2008, the M.A.Sc. degree from Xi'an Jiaotong University, Xi'an, China, in 2012, and the Ph.D. degree from Ryerson University, Toronto, ON, Canada, in 2017, all in electrical engineering.

From 2012 to 2014, he was with Delta Power Electronics, Nanjing, China, as an R&D Engineer. In 2018, he joined Lakehead University, Thunder Bay, ON, Canada, where he is currently an Associate Professor. His research is focused on innovative power conversions and controls for high-power applications, such as renewable energies, drives, and electric vehicles.

Yunwei (Ryan) Li (Fellow, IEEE) received the B.Sc. degree from Tianjin University, Tianjin, China, in 2002, and the Ph.D. degree from the School of Electrical and Electronic Engineering, Nanyang Technological University, Singapore, in 2006.

In 2005, he was a Visiting Scholar with Aalborg University, Denmark. From 2006 to 2007, he was a Postdoctoral Research Fellow with Ryerson University, Canada. In 2007, he also worked with Rockwell Automation Canada before he joined the University of Alberta, Canada, in the same year. Since then, he has been with the University of Alberta, Edmonton, ON, Canada, where he is currently a Professor and Acting Department Chair. His research interests include distributed generation, microgrid, renewable energy, high-power converters, and electric motor drives.

Dr. Li was a recipient of the Nagamori Foundation Award in 2022 and the Richard M. Bass Outstanding Young Power Electronics Engineer Award from the IEEE Power Electronics Society (PELS) in 2013. He currently serves as the Vice President for Products of IEEE PELS. He was the Editor-in-Chief for IEEE TRANSACTIONS ON POWER ELECTRONICS LETTERS in 2019–2023. He also served as an Associate Editor for IEEE TRANSACTIONS ON POWER ELECTRONICS, IEEE TRANSACTIONS ON INDUSTRIAL ELECTRONICS, IEEE TRANSACTIONS ON SMART GRID, and *IEEE Journal of Emerging and Selected Topics in Power Electronics*. He was the General Chair of the IEEE Energy Conversion Congress of Exposition in 2020. He is the AdCom Member at Large for IEEE Power Electronics Society (PELS) in 2021–2023. He is recognized as a Clarivate Highly Cited Researcher.